



## Evidence of a chlorophyll “tongue” in the Malacca Strait from satellite observations

Samiran Mandal<sup>a,\*</sup>, Nibedita Behera<sup>a,b</sup>, Avijit Gangopadhyay<sup>c,a,d</sup>, R. Dwi Susanto<sup>e</sup>, Prem Chand Pandey<sup>d</sup>

<sup>a</sup> School of Earth, Ocean and Climate Sciences, Indian Institute of Technology Bhubaneswar, India

<sup>b</sup> Indian National Centre for Ocean Information Services, India

<sup>c</sup> School for Marine Science and Technology, University of Massachusetts, Dartmouth, USA

<sup>d</sup> Centre for Oceans, Rivers, Atmosphere and Land Sciences, Indian Institute of Technology Kharagpur, India

<sup>e</sup> Department of Atmospheric and Oceanic Science, University of Maryland, MD, USA

### ARTICLE INFO

#### Keywords:

Malacca Strait  
Chlorophyll-a concentration  
Ekman dynamics  
Chlorophyll-a tongue  
Coastal upwelling  
MJO

### ABSTRACT

Remotely sensed surface chlorophyll-a concentration from the Moderate Resolution Imaging Spectroradiometer (MODIS) unveils signatures of a “tongue” like feature extending into the Malacca Strait from the west of Malaysia. A threefold increase of chlorophyll-a amplitudes is observed in the strait during the northeast monsoon (December–February) compared to the lowest values during the southwest monsoon (May–September). This seasonal variability of chlorophyll-a is linked with the seasonal variabilities of the meridional component of Ekman mass transport ( $M_y$ ), sea surface temperature (SST), wind stress curl, and the sea surface height anomaly (SSHA). A multiple regression analysis indicates that the monsoonal winds and SST are the dominant contributors to the chlorophyll-a variability in the strait. The role of SSHA is limited to the presence of a seasonal cyclonic eddy in the strait during December–February and its associated upwelling. The monsoonal winds associated with the active phase of Madden Julian Oscillation (MJO) events during November induced strong coastal upwelling along the west coast of Malaysia. Later, strong upwelling associated with both wind-induced coastal upwelling and open ocean upwelling due to wind stress curl is observed in the strait during December–February, which is also well supported by the entrainment of cold and saline waters from the subsurface and advection of colder SST within the strait. The advection of higher chlorophyll-a in the north-westward extension of the “tongue” off the west coast of Malaysia during December – February is attributed to the Ekman mass transport due to higher wind stress. On the other hand, lower chlorophyll-a during May–September is due to the negative wind stress curl and downwelling. Rectified wavelet analysis shows higher correlations of chlorophyll-a variability with the active phases of the MJO events than with the ENSO and IOD events, indicating substantial impacts of the MJO events in the Malacca Strait.

### 1. Introduction

The Malacca Strait (MS) is a narrow extension of the Andaman Sea (AnS) at the south, covering the region between 96–103°E and 2–8°N. It is the most popular international sea route connecting the Indonesian Seas (Natuna Sea and Karimata Strait), the South China Sea (SCS), and the Indian Ocean (Fig. 1a). To the south of the SCS, lies the Natuna Sea, which is connected to the Java Sea through the Karimata Strait. The biological activity in the northern Indian Ocean is mainly influenced by

the seasonally reversing monsoonal winds: the south-westerly (north-easterly) winds during May–October (November–February) with strong and steady wind conditions in July–August (January) (Joo and Samah, 2004). For the first time, the ship datasets were used to characterize the surface circulation variability in the MS, which is mostly north-westward throughout the year due to the prominent sea level gradients between the two ends of the strait, with a descending slope towards the AnS (Wrytki, 1961). The same study indicated the importance of investigating the water mass properties in terms of physicochemical

\* Corresponding author at: Ocean Analysis and Modeling Laboratory, School of Earth, Ocean, and Climate Sciences, Indian Institute of Technology Bhubaneswar, Argul Campus, Jatni, Odisha 752050, India.

E-mail address: [sm18@iitbbs.ac.in](mailto:sm18@iitbbs.ac.in) (S. Mandal).

<https://doi.org/10.1016/j.jmarsys.2021.103610>

Received 7 December 2020; Received in revised form 6 July 2021; Accepted 9 July 2021

Available online 15 July 2021

0924-7963/© 2021 Elsevier B.V. All rights reserved.

parameters in the strait. During the northeast monsoon (NEM, November–February), the throughflow towards the Java Sea is more substantial compared to those during the southwest monsoon (SWM, May–September) (Susanto et al., 2013; Wei et al., 2019). The volume transport through the MS towards the Indian Ocean is small ( $-0.12$  Sv) (Wang et al., 2019). During the NEM, the water mass properties in the SCS and the southern part of MS are similar (Pang and Tkalich, 2003). In contrast, Ibrahim and Yanagi (2006) have shown the intrusion of saline waters from the AnS into the MS during the SWM. Recent modeling studies by Haditjar et al. (2019) have shown that the volume transport is always towards the Indian Ocean during both the monsoon seasons, with the highest transport during the NEM (in January) than during the SWM (in July).

On the other hand, other studies in the MS have focused on the characteristics of tides and the associated physical processes. The M2 tidal currents are observed with amplitudes of  $\sim 60$  cm  $s^{-1}$  at the southern part of the strait, which further increases due to the interactions with shallow and complex bathymetry features (Wrytki, 1961; Chen et al., 2014). Also, a virtual amphidromic point has been identified in the MS, which influences the circulation pattern as well

(Rizal, 2000). The circulation pattern in the strait is controlled by the combined effects of winds, tides, and surface heat fluxes (Rizal et al., 2010, 2012). However, a recent study by Chen et al. (2014) have attempted to distinguish the wind-driven circulation from the tidal-driven flow and argued on the dominance of wind-driven circulation even if the tidal currents are strong (Rizal, 2000). Also, earlier studies have reported the modulation of the monsoonal winds by the Madden–Julian Oscillations (MJO) and mesoscale convective systems over the Maritime Continent (Chang et al., 2005; Salahuddin and Scott, 2011). As compared to the AnS (Mandal et al., 2020), the biological activity, as well as the circulation pattern in the MS, have not been explored as it is one of the poorly observed regional straits.

The chlorophyll-a variability in the MS has not received much attention except a few studies, which have focused on the quantification of chlorophyll-a trends until 2010 and related those to the positive and negative phases of El-Nino Southern Oscillation (ENSO) and Indian Ocean Dipole (IOD) events (Siswanto and Tanaka, 2014; Isa et al., 2020). Earlier studies have reported cold waters with lower salinity either using ship observations or numerical models. Satellite observations have typically shown the presence of a “tongue” like feature in the

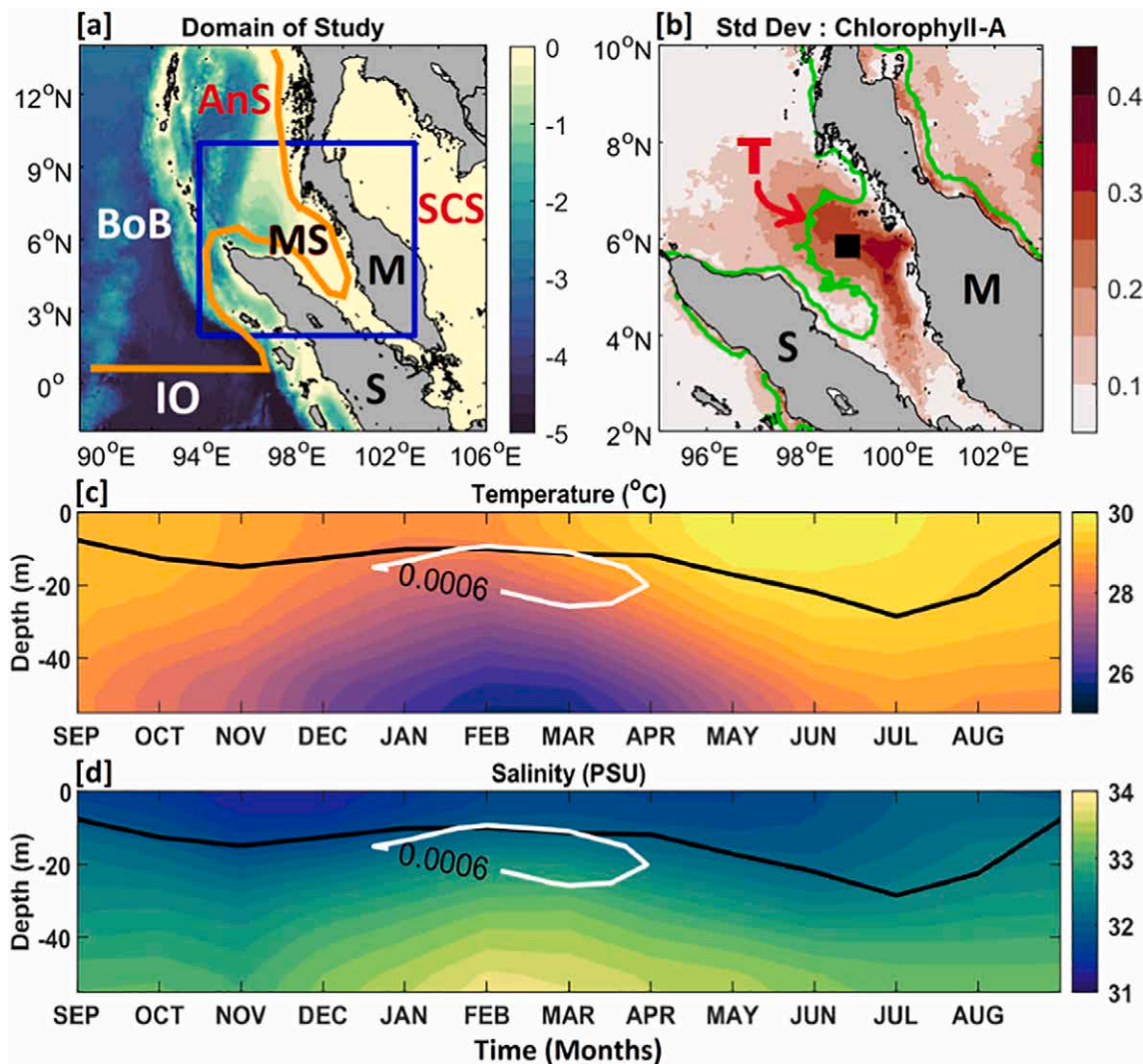


**Fig. 1.** (a) The shaded background represents the bathymetry from ETOPO2 (in km). The region marked in the thick blue line is the domain of interest. AnS, BoB, IO, M, MS, S, and SCS denote the Andaman Sea, Bay of Bengal, Indian Ocean, Malaysia, Malacca Strait, Sumatra, and South China Sea, respectively. The orange line displays the Kelvin waves pathway. (b) The standard deviation of chlorophyll-a concentration from MODIS during 2007–2018. The green contour ( $-0.2$   $mg\ m^{-3}$  in logarithm scale) denotes the chlorophyll-a averaged during December–February. The subsurface variations of climatological (c) temperature and (d) salinity from WOA18, with the mixed layer depth (m, black contour) and Brunt–Väisälä frequency ( $N^2$ ) ( $s^{-2}$ , white contour) at the black dot in panel ‘b’. (For interpretation of the references to colour in this figure legend, the reader is referred to the web version of this article.)

strait during the northeast monsoon period. This pattern is shown in Fig. 1b from the standard deviation of chlorophyll-a from 12 years (2007–2018) of data. Thus, the present article is aimed to identify this upwelling hotspot in the MS, to study its spatial variability, and further investigate the physical mechanisms responsible for the evolution of the chlorophyll-a “tongue” using the multiple sets of remotely-sensed satellite datasets at the seasonal time scale. Moreover, the chlorophyll-a variability during the different phases of MJO, ENSO, and IOD events is also investigated.

## 2. Data and methodology

In the present study, the monthly chlorophyll-a concentration derived from the Moderate Resolution Imaging Spectroradiometer (MODIS) Aqua, available at ~4 km spatial resolution, is used to investigate the surface chlorophyll-a concentration distribution in the MS (source: <https://oceancolor.gsfc.nasa.gov/>). The daily level-4 SST data (at 5 km) from the Operational Sea Surface Temperature and Sea Ice Analysis (OSTIA) data product is obtained from the Group for High-Resolution Sea Surface Temperature (GHRSSST) at the UK Met Office (source: <https://podaac.jpl.nasa.gov/GHRSSST>). The monthly gridded 10 m winds from the Advanced Scatterometer (ASCAT) are extensively used to examine the surface winds variability in the domain, which are accessible at the spatial resolution of 25 km (Mandal et al., 2018a, 2018b) (source: <http://apdrc.soest.hawaii.edu/datadoc/ascats.php>). The monthly merged altimeter-derived sea surface height anomaly (SSHA) data, available at a spatial resolution of 25 km, from the Archiving, Validation, and Interpretation of Satellite Oceanographic (AVISO) altimetry are used to derive the geostrophic currents and further diagnosed the surface circulation variability in the MS (source: <http://marine.copernicus.eu/>). Furthermore, the improved monthly temperature and salinity data (both at surface and subsurface) from the World Ocean Atlas 2018 (WOA18), available at a spatial resolution of 25 km, are used to support the implications (source: <https://www.ncei.noaa.gov/access/world-ocean-atlas-2018/>). The mixed layer depth (MLD) is calculated as the depth at which the density is higher than the surface density by a quantity equivalent to a temperature drop of 1.0 °C (Jana et al., 2015). Note that the entire study is based on climatology data (averaged during 2007–2018) from multiple remote sensing observation platforms.

The possible influences of the climate phenomena associated with the ENSO, IOD, and MJO events on the long-term variations of chlorophyll-a concentration in the domain are also investigated at multiple time scales. The Dipole Mode Index (DMI) is acquired from the Japan Agency for Marine-Earth Science and Technology to investigate the variations associated with the IOD events in the Indian Ocean during 2007–2018 (source: <http://www.jamstec.go.jp/frsgc/research/d1/iod/dmi.html>). The Nino3.4 index is acquired from the Climate Prediction Center of the National Oceanic and Atmospheric Administration during the same period of study (source: <http://www.cpc.ncep.noaa.gov/data/indices/sstoi.indices>). Further, to analyze the variabilities associated with the intraseasonal oscillations, the daily Real Time Multivariate MJO (RMM) indices are acquired from the Bureau of Meteorology, Australia (source: <http://www.bom.gov.au/cli/mate/mjo/>).

## 3. Geographical setting (Hydrography) of the Malacca Strait

The MS to the south of the AnS is a narrow, funnel-shaped region between the Malaysia Peninsula and Sumatra Island with shallow bathymetry (<500 m). The wide continental slope gradually narrows to the south of the strait with a sharp decline in the depth (nearly 10–40 m) to indicate the dense tidal flats. Both shallow bathymetry and channel geometry play a significant role in the amplification of tidal currents (van Maren and Gerritsen, 2012). Note that the water depth increases abruptly from 500 m to 1000 m near 6°N (Fig. 1a). The rivers like the

Klang, Langat, Perak, and Selangor are the principal sources of freshwater discharge during the early northeast monsoon (November–December) (Hii et al., 2006). Owing to the absence of in situ observations in the domain, the climatological temperature and salinity data are used to investigate the local upper ocean variability (Fig. 1c and d).

The signatures of the four phases of the coastally trapped Kelvin waves (cKWs) are prominently observed in the strait, with the first upwelling phase during January–March, followed by the first downwelling phase during April–June, the second upwelling phase during July–September, and the second downwelling phase during October–December (Rao et al., 2010) (orange line in Fig. 1a). The climatological temperature in the subsurface varies in the range 26–31 °C showing higher temperatures (>30 °C) during SWM than during the NEM (<29 °C) above the MLD (Fig. 1c). Similarly, salinity varies between 30.5 and 34 psu within the water column, with comparatively lower salinity (~30.5 psu) during October–December in the upper ocean (Fig. 1d). The entrainment of the cold waters is observed well from the subsurface temperature and salinity profiles during the NEM phase, which is associated with the shallow MLD (~15 m) during December–February and mixed layer deepening (~30 m) during May–September (black contour in Fig. 1c and d). Furthermore, a stratified and stable water column is observed from Brunt–Väisälä frequency ( $N^2$ ) distribution (white contour in Fig. 1c and d) during the post northeast monsoon period (January–March).

## 4. Results

In this section, the seasonal variability of chlorophyll-a concentration in the MS is first investigated, followed by presenting the evidence of a chlorophyll-a “tongue” in subsection 4.1. Seasonal variability of other physical parameters (SST, winds, and SSHA) in the MS are discussed in subsection 4.2. An investigation of the multiple dynamical factors influencing the chlorophyll-a variability is then described in subsection 4.3.

### 4.1. Variability of chlorophyll-a in the Strait

The spatial distribution of the standard deviation of the logarithm of chlorophyll-a concentration indicates the highest variations along the west coast of Malaysia with magnitudes of 0.32 mg m<sup>-3</sup>. This high amplitude region is observed to spread north-westward off the strait in the shape of a “tongue” (green contour in Fig. 1b). Surface climatological chlorophyll-a maps from MODIS data averaged over 2007–2014 are shown in Fig. 2. Although the highest amounts of chlorophyll-a are observed along the southern part of the MS (south of 4°N) throughout the year, significant inter-seasonal variability is also evident with higher chlorophyll-a concentration along the eastern side and in the center of the strait to the north of 4°N during the NEM, in contrast to lower concentration during the SWM (Fig. 2).

Interestingly, the highest values of chlorophyll-a (~0.25 mg m<sup>-3</sup>) during December–February shows the prominent signature of a “tongue” of chlorophyll-a, which extends into the strait starting from the west of Malaysia (Fig. 2c). The generation of this tongue is observed during November, which intensified later during December–February and then disappeared in April (Fig. 2b-d). The plausible factors for the generation and evolution of the chlorophyll-a “tongue” are analyzed next in terms of the wind-induced curl, local upwelling, SST and SSHA anomaly variability.

### 4.2. Variability of winds, SST, and SSHA in the strait

The MS experiences a seasonal reversal of the monsoonal winds; the south-westerlies with a wind speed of ~1.75 m s<sup>-1</sup> during May–September (SWM) and north-easterlies with a higher wind speed of nearly 4.50 m s<sup>-1</sup> during November–February (NEM). A substantial seasonality in the wind stress is also observed in the domain from the ASCAT winds

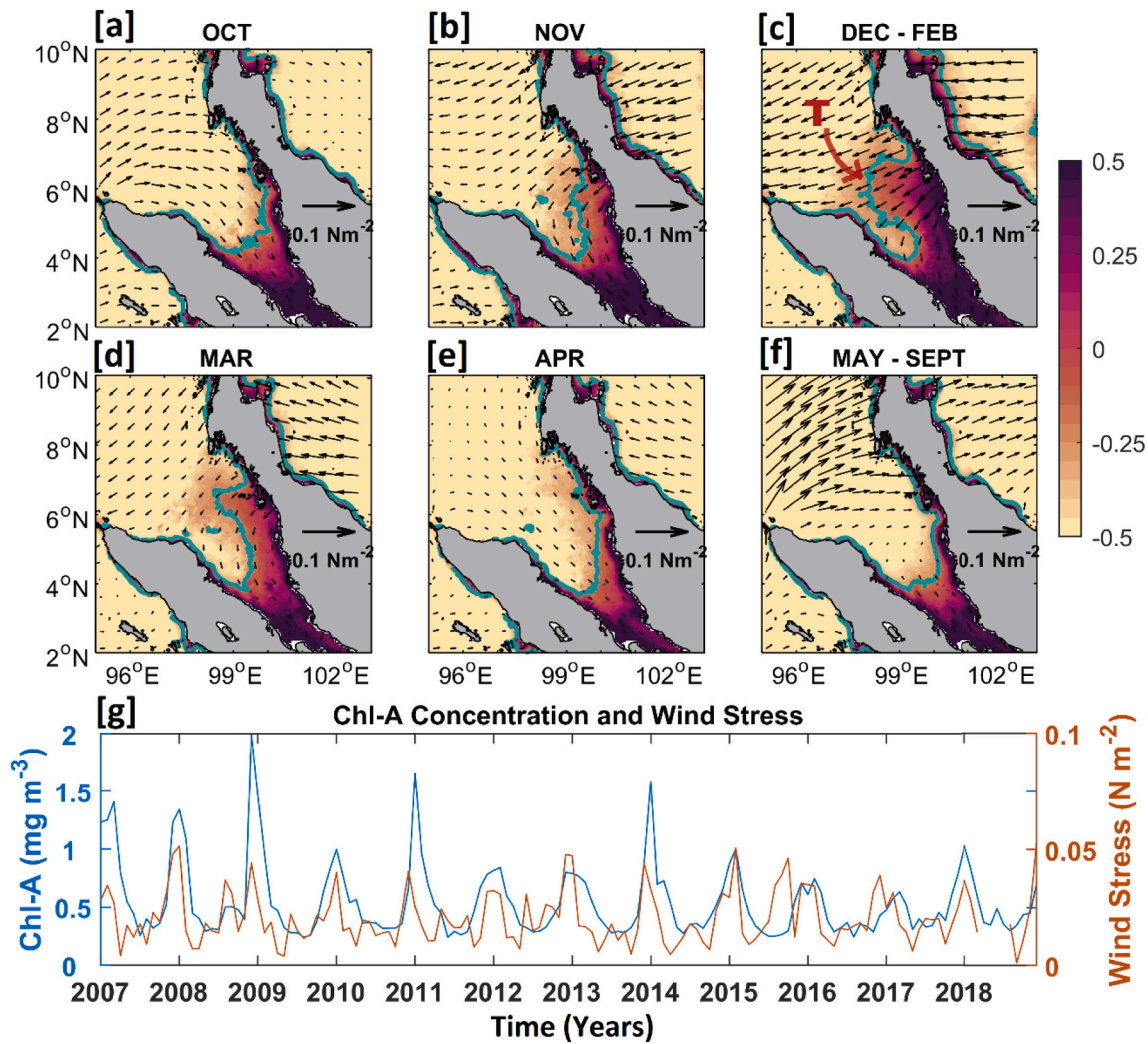


**Fig. 2.** (a) Monthly surface chlorophyll-a maps (in logarithm scale, in  $\text{mg m}^{-3}$ ) during (a) October, (b) November, (c) December–February, (d) March, (e) April, and (f) May–September from MODIS chlorophyll-a data (shaded background), overlaid by surface wind stress during 2007–2018. The cyan contour indicates the tongue of chlorophyll-a ( $\sim 0.2 \text{ mg m}^{-3}$ ). (g) The time evolution of box-averaged chlorophyll-a concentration (in  $\text{mg m}^{-3}$ ) with wind stress magnitude (in  $\text{N m}^{-2}$ ) during 2007–2018. (For interpretation of the references to colour in this figure legend, the reader is referred to the web version of this article.)

averaged during 2007–2018 (Fig. 2). Monthly mean winds indicate lower wind stress ( $\sim 0.01 \text{ N m}^{-2}$ ) inside the strait (mostly south of  $7^\circ\text{N}$ ) throughout the year, except during November–February when the highest wind stress is observed ( $\sim 0.05 \text{ N m}^{-2}$ ) (Fig. 2c). The alongshore winds inside the strait during the NEM (Fig. 2b–d) are more robust than those during the SWM phase, which further leads to the intense positive wind stress curl in the domain. The temporal variation of the box-averaged chlorophyll-a concentration during 2007–2018 indicates the highest chlorophyll-a magnitudes in December every year (Fig. 2g). Also, stronger winds are observed over the MS during the NEM along with the highest wind stress magnitudes ( $\sim 0.05 \text{ N m}^{-2}$ ) during the concurrent time and have a reasonable correlation of 0.58 ( $p$ -value  $< 0.001$ ) with chlorophyll-a concentration (Fig. 2g).

Fig. 3 shows the seasonal evolution of surface wind stress curl spatial maps overlaid by chlorophyll-a concentration in the strait (magenta contours). With the onset of NEM in mid-October, the wind stress curl starts increasing with the increase in wind stress in the domain. The wind stress curl attains its maximum ( $2 \times 10^{-7} \text{ N m}^{-3}$ ) during November–February (Fig. 3c), indicating strong upwelling in the domain along with the prominent signatures of a “tongue” extending north-westward from the west coast of Malaysia, which is well evident from the higher values of chlorophyll-a during the same time period (Fig. 2c). However, the wind stress curl has reduced to  $-2 \times 10^{-7} \text{ N m}^{-3}$

during May–September (SWM), indicating downwelling (Fig. 3f), which is well supported by the lower chlorophyll-a concentrations as well as the absence of chlorophyll-a “tongue” (Fig. 3f).

The temporal variability of both the wind stress and its curl indicates the highest values during November–February, which points to the positive influence of winds for the upwelling and the generation of chlorophyll-a “tongue”. Moreover, the temporal variability of the meridional component of Ekman mass transport indicates the highest values during December. Thus, both the wind stress curl (through open ocean upwelling) and the meridional component of the Ekman mass transport (through coastal upwelling) play a significant role in the chlorophyll-a variability in the strait.

Seasonal variations in sea-level anomalies and surface circulation patterns in the MS are investigated next from the altimetry-derived climatological SSHA, seasonally averaged during 2007–2015 (Fig. 4). The upwelling and downwelling phases of the cKW are well captured in the northern part of the MS, with the highly intensified first upwelling phase (January–March) and first downwelling phase (May–August) of the cKWs, and weak second upwelling (September) and downwelling (October–December) phases (Fig. 4). The signatures of a well-developed cyclonic eddy are well evident in the strait from the surface circulation patterns during the first upwelling phase of the cKWs (Fig. 4c and d). In contrast, an anticyclonic eddy is observed during May–September

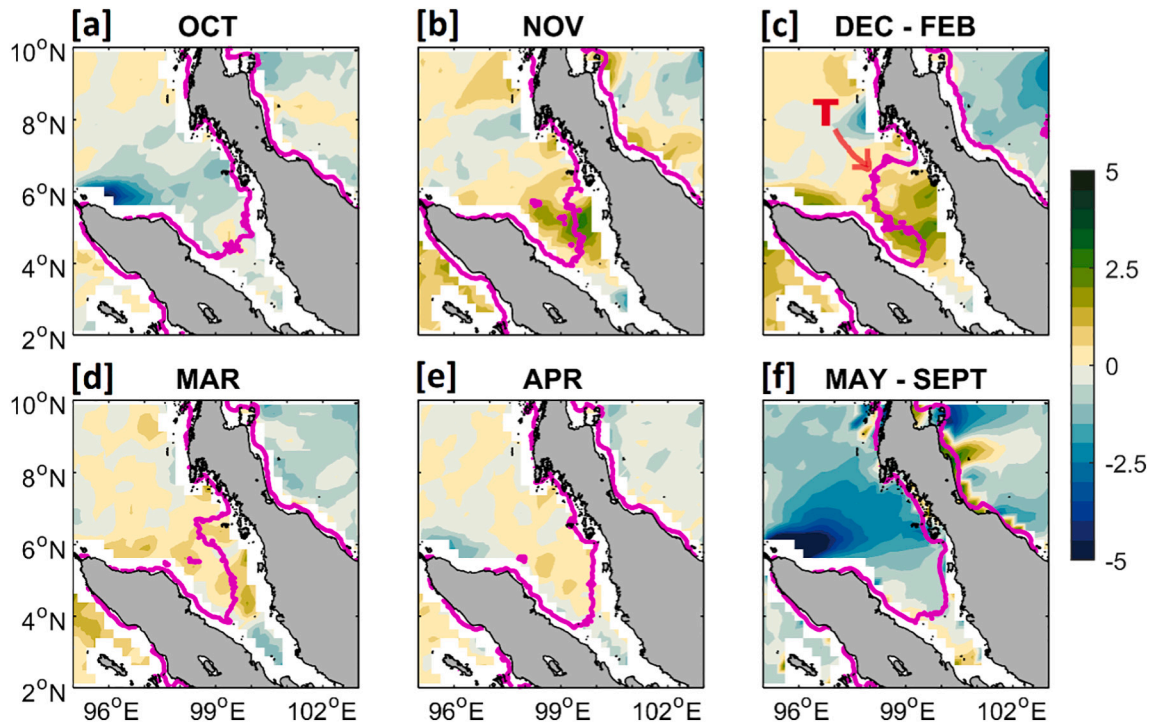


Fig. 3. Same as Fig. 2, but for surface wind-stress curl (in  $\times 10^{-7} \text{ N m}^{-3}$ ) averaged during 2007–2018. The magenta contour indicates the chlorophyll “tongue”. (For interpretation of the references to colour in this figure legend, the reader is referred to the web version of this article.)

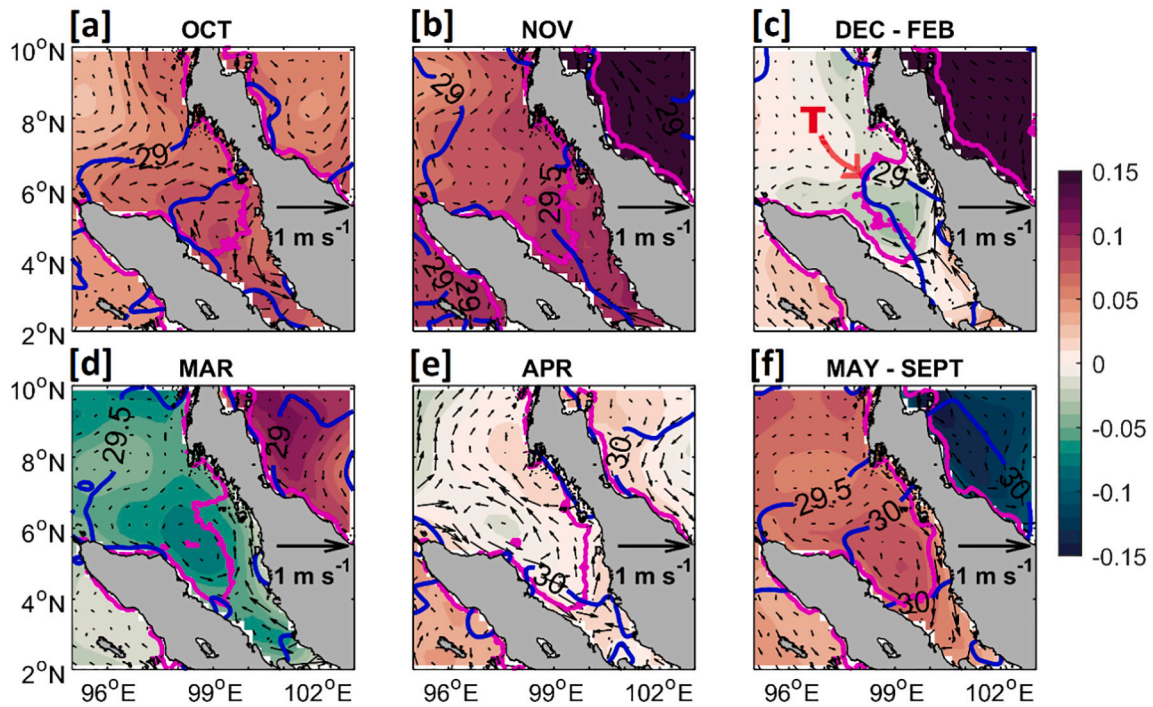


Fig. 4. Same as Fig. 2, but for sea surface height anomaly (SSHA) from AVISO altimetry data (shaded background), overlaid by geostrophic currents averaged during 2007–2015. The magenta contour indicates the tongue of chlorophyll ( $-0.2 \text{ mg m}^{-3}$  in logarithm scale). The blue contour shows the variations of sea surface temperature. (For interpretation of the references to colour in this figure legend, the reader is referred to the web version of this article.)

during the SWM, associated with the first downwelling phase of cKW (Fig. 4f). At the mesoscale, cyclonic (anticyclonic) eddies can drive upwelling (downwelling) and are subsequently associated with depressed (elevated) sea surfaces (Chelton et al., 2011). To further represent the chlorophyll-a variability in the strait, the box-averaged log-transformed MODIS chlorophyll-a concentration and SSHA during

2007–2016 are correlated with a correlation coefficient of  $-0.36$ , i.e., the higher (lower) chlorophyll-a concentration is associated with negative (positive) sea level anomalies during the NEM (SWM).

SST is one of the key physical parameters in the upper ocean, which can be related to the upper ocean stratification, variations in the air-sea fluxes, surface circulation features, and other oceanic processes. Higher

SST (nearly 30.5 °C) is observed during May–September, whereas comparatively lower SST (nearly 29 °C) is observed during December–February along the west coast of Malaysia in the MS. Moreover, the entrainment of the cold and saline waters from the subsurface is also apparent from the climatological temperature and salinity profiles during December–February along with the uplifting of the MLD and isotherms (Fig. 1c and d). This is well supported by a significant drop in SST from 30.5 °C to 29 °C in the strait. The comparison of box-averaged chlorophyll-a concentration and SST indicate a high correlation of  $-0.65$  (with  $p$ -value  $<0.001$ ) in most of the areas in the domain, i.e., the higher (lower) concentrations of chlorophyll-a are associated with colder (higher) SST during the NEM (SWM) (Fig. 4).

This entrainment feature concomitant to the presence of a cyclonic eddy may indicate an eddy-induced upwelling in the strait. Moreover, a freshwater influx from the major rivers is also observed along the west coast of Malaysia during the NEM, indicating that the cold SST plume is in-phase with the chlorophyll-a “tongue” (Fig. 4c). Earlier studies in the strait have reported the highest river discharge during October–November (approx.  $400 \text{ m}^3 \text{ s}^{-1}$ , source: <http://www.sage.wisc.edu/riverdata>), which may also carry a significant amount of nutrients from the land into the MS (Hii et al., 2006). Also, Tan et al. (2006) have shown that the unique topology of MS, i.e., the mountain ranges of Malaysia and Sumatra, may act as the barrier to the monsoonal winds, which can impact both the downwelling and upwelling phenomena at the northern part of MS during different SWM and NEM, respectively. It can be speculated that all the physical parameters (winds, SST and SSHA) may be involved in the seasonal variability of chlorophyll-a in the strait. Thus, the following section focuses mainly on investigating the factors influencing the chlorophyll-a variability in the domain.

#### 4.3. Dynamical factors controlling chlorophyll-a variability

The seasonal variability of chlorophyll-a and its forcing parameters such as the wind stress curl, SST, Ekman mass transport, and SSHA is presented in Fig. 5. Twelve years (2007–2018) of data for each variable (e.g., Fig. 2g) is averaged to determine the seasonal cycles in Fig. 5 along with the standard errors (shaded), which clearly shows the highest chlorophyll-a concentration during December–February. The direct correlation coefficients between chlorophyll-a and other factors are calculated from their normalized monthly anomalies to investigate their inter-relationship. Exposure to light and nutrients are the major factors to control the chlorophyll-a concentration and phytoplankton growth in the strait (Chaturvedi et al., 1998). Significantly strong correlations are observed between chlorophyll-a and SST in the MS (Fig. 5), especially along the coastal regions of west Malaysia, with a high correlation

coefficient of  $-0.82$  ( $p$ -value  $<0.001$ ). Note that both the chlorophyll-a concentration and SST show a dominant seasonality with opposing phases, and the highest correlation ( $-0.82$ ) is reached without any lags.

Wind-driven mixing is another important phenomenon, which can positively result in the entrainment of cold waters from the subsurface in the open ocean or coastal upwelling in the MS, leading to the high chlorophyll-a concentration at the surface. In this domain, strong seasonality is observed in both the meridional component of Ekman mass transport ( $M_y$ ) and wind stress curl, with direct correlation coefficients of 0.95 and 0.77 ( $p$ -value  $<0.001$ ), respectively. However, a significantly higher correlation (0.82) is observed with chlorophyll-a when wind stress curl leads by one month. Moreover, a lower correlation with the wind stress curl indicates lower contributions from eddy-induced upwelling to the high chlorophyll-a concentration. It is interesting to note that the temperature and salinity profiles indicate upwelling in the strait. On the other hand, a comparatively high correlation with  $M_y$  indicates strong coastal upwelling features along the west coast of Malaysia during December–February compared to eddy-induced upwelling in the strait.

The SSHA and associated circulation patterns are also related to the local dynamics, like the eddy distribution and vertical transport of waters. The north-easterlies during the NEM induce positive wind stress curl, which leads to the entrainment of dense waters from the subsurface, resulting in low sea levels (negative SSHA) and higher chlorophyll-a concentration (Fig. 5). The south-westward winds during the NEM are favorable to drive a mesoscale cyclonic eddy in the MS during December–March, leading to high chlorophyll-a at the surface, well evident from negative correlation ( $-0.47$ ) between chlorophyll-a and SSHA (Fig. 5).

A Hovmöller diagram for the monthly averaged chlorophyll-a concentration is shown in Fig. 6, overlaid with contours of wind stress curl, SST, and SSHA, along a longitudinal section at 99.5°E. The seasonal variability indicates the coevolution of chlorophyll-a, winds, and SST, with the generation of the chlorophyll-a tongue in mid-November and persisting in the MS until early March. The tongue has the maximum intensity during December–February extends from the west coast of Malaysia between 5°N to 7°N.

### 5. Quantifying the relative roles of factors in controlling chlorophyll-a variability

It is clear from the above results that the seasonal variations in chlorophyll-a in the strait are significantly correlated with multiple dynamical factors, such as the winds and SST, and in a limited way with SSHA. In this section we present (i) a multiple regression analysis to quantify the relative contributions of these factors towards the seasonal variability of chlorophyll-a, and (ii) an indirect inference of the impact of MJO on the intraseasonal variability of chlorophyll-a using rectified wavelet analysis technique.

#### 5.1. Multiple regression analysis (quantifying seasonal variability)

The wind played an important role in mixing the water column followed by vertical transport of the nutrients, which would impact the chlorophyll-a variability. The associated upwelling phenomenon brought cold and dense waters to the surface, which decreased the SST and depressed the sea levels, thereby cooling the surface. At the same time, the high chlorophyll-a concentrations are associated with lower SSTs and SSHAs, and strong wind stress curl due to strong winds during NEM. Thus, it is evident that the MS experiences a strongly coupled seasonal chlorophyll-a variability. The strong intercorrelations revealed that high (low) wind stress curl and Ekman mass transport ( $M_y$ ) could induce enhanced (reduced) chlorophyll-a in the domain. Higher significance levels are observed without any lags, indicating that the Ekman mass transport, wind stress curl, and SST have simultaneously impacted the chlorophyll-a levels in the domain. However, the intercorrelations

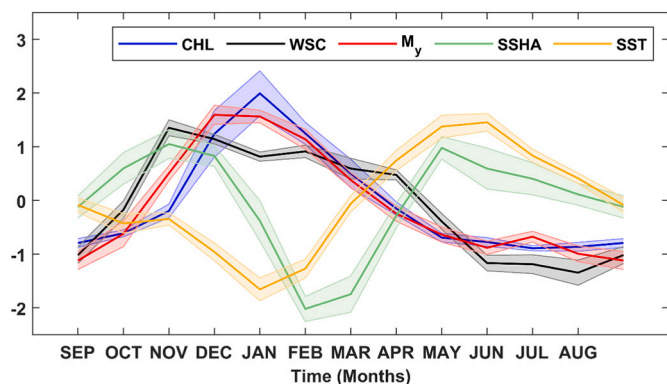


Fig. 5. Seasonal variability of normalized chlorophyll-a (CHL), wind stress curl (WSC), meridional component of Ekman mass transport ( $M_y$ ), sea surface height anomaly (SSHA), and sea surface temperature (SST) averaged during the period 2007–2018. The shaded areas show the standard error of mean for each time series.

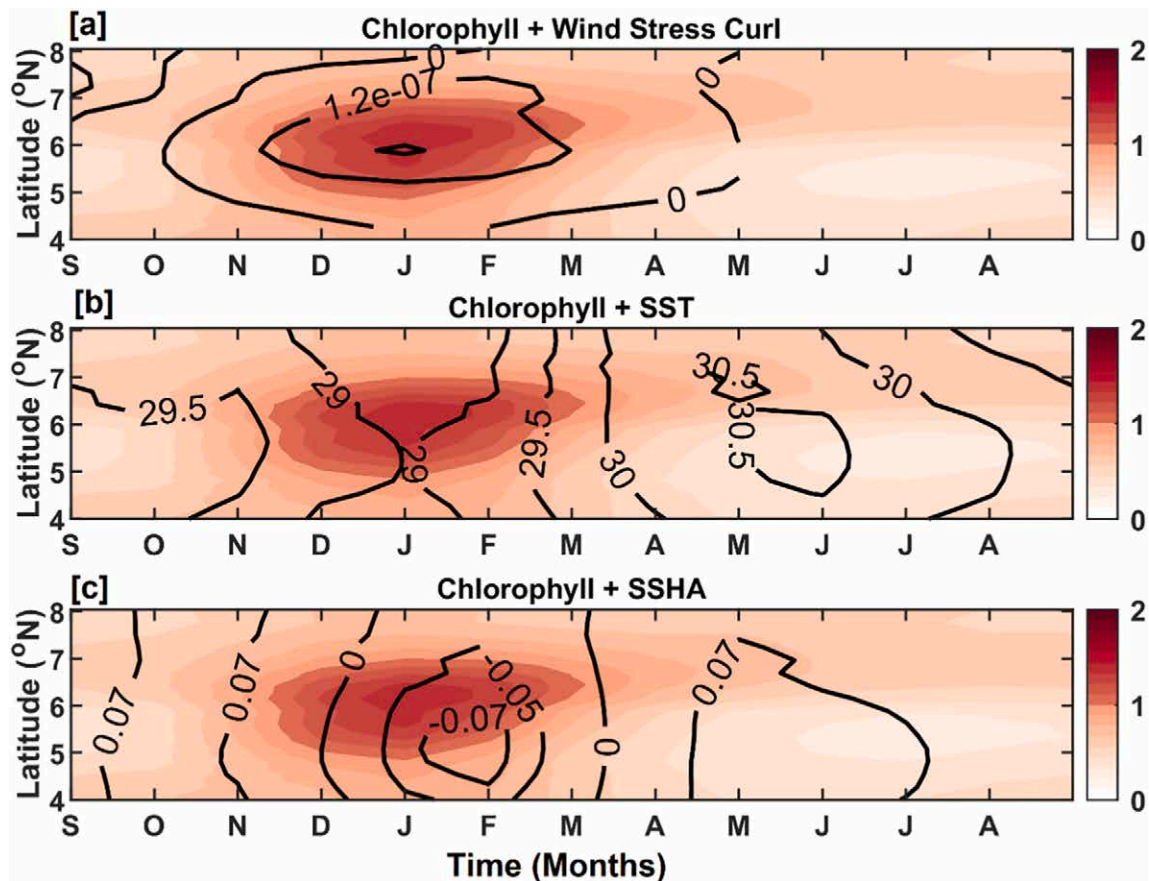


Fig. 6. The Hovmöller diagram for climatological chlorophyll-a concentration (in logarithm scale) (shaded background) along the longitudinal transect (at 99.5°E) in all the panels. Overlaid black contours represent climatological (a) wind stress curl ( $\text{N m}^{-3}$ ), (b) SST ( $^{\circ}\text{C}$ ), and (c) SSHA (m) during the period 2007–2018 in the three panels.

made it difficult to distinguish the individual impact of each factor. So, the contribution of the various factors is quantified in terms of multiple regression between the different factors (Table 1).

Multiple regression analysis of the parameters has been carried out on a seasonal time scale for three different combinations as follows: (i) chlorophyll-a with all other parameters (Model A), (ii) chlorophyll-a with the meridional component of Ekman mass transport, SST and SSHA (Model B), and (iii) chlorophyll-a with wind stress curl, SST and SSHA (Model C) (Table 1). For the first case, the meridional component of Ekman mass transport-induced coastal upwelling is the dominant forcing (at 99% significance level) responsible for the high chlorophyll-a concentration in the domain, followed by the combined influence of wind stress curl and SST. However, the SSHA contributes the least to the higher chlorophyll-a concentration in the domain. To distinguish the

Table 1

Multiple regression analysis of the independent variable chlorophyll-a (CHL) with respect to the dependent variables, wind stress curl (WSC), meridional component of Ekman mass transport ( $M_y$ ), sea surface height anomaly (SSHA), and sea surface temperature (SST) averaged during the period 2007–2018.

Models	SST	$M_y$	WSC	SSHA	Other Factors
A	-0.09	1.03*	-0.23	-0.17	$-8.96 \times 10^{-16}$
B	-0.10	0.82*	NA	-0.18	$-9.72 \times 10^{-16}$
C	-0.47*	NA	0.40	-0.19	$-3.39 \times 10^{-15}$

Note: 1. Model A denotes  $\text{CHL} = f(\text{WSC}, M_y, \text{SST}, \text{and SSHA})$ .

2. Model B denotes  $\text{CHL} = f(M_y, \text{SST}, \text{and SSHA})$ .

3. Model C denotes  $\text{CHL} = f(\text{WSC}, \text{SST}, \text{and SSHA})$ .

The beta coefficients marked '\*' are 95% significant ( $p$ -value  $< 0.05$ ). 'NA' stands for not available

relative contributions from SST and wind stress curl, two different multiple regressions have been performed (Table 1). Moreover, the multiple regression on the second set of parameters again indicates that the meridional component of Ekman mass transport induced upwelling is the dominant forcing than the SST and SSHA. In contrast, it is interesting to note that SST plays a significant role in comparison to the wind stress curl in the domain in the third case, when the dependency of chlorophyll-a on wind stress curl, SST, and SSHA is investigated (Table 1).

We note in passing that, a similar multiple regression analysis is also performed on the interannual time scale, but the results are not statistically significant due to limited number of years (12) and are not discussed. Furthermore, the impact of large-scale climate phenomena has also been investigated to analyze the long-term variabilities in chlorophyll-a in the MS, a robust spatial comparison of chlorophyll is performed with the ENSO and DMI indices. The negative correlation with the IOD and ENSO events indicates the higher chlorophyll-a concentration during the La-Nina years (correlation nearly  $-0.10$ ) and the negative IOD years (correlation nearly  $-0.15$ ) (Fig. 7a and b). Note that ENSO is weak in northern Sumatra and Malay (Aldrian and Susanto, 2003). Although the interannual variations in Ekman dynamics in the MS are weak, the same is comparatively stronger along the Java coast (Wirasatriya et al., 2020) and other Indonesian Seas (Setiawan et al., 2019, 2020).

## 5.2. Wavelet analysis (inferring intraseasonal variability)

The equatorial zonal winds predominantly influence the Indonesian Throughflow (ITF) region and show significant signatures of the active

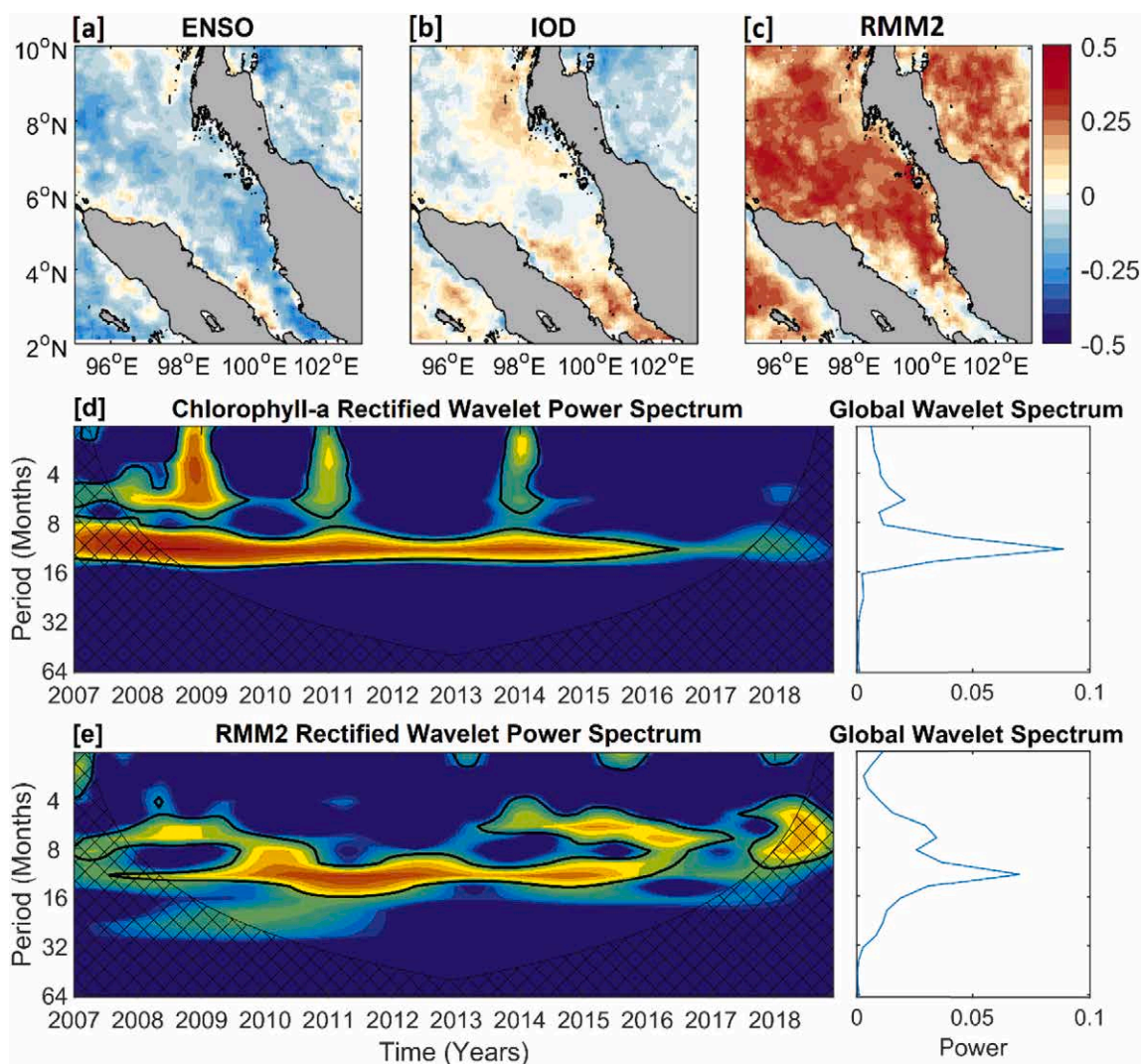


**Fig. 7.** Spatial correlation maps of monthly chlorophyll concentration with the (a) ENSO, (b) IOD, and (c) MJO indices during 2007–2018. Rectified wavelet power spectrum and corresponding global wavelet spectrum of (d) chlorophyll-a concentration and (e) RMM2 index during 2007–2018. Note that the cross-hatched regions in the rectified wavelet power spectra are outside the “cone of influence”. The significant periods with greater than 95% confidence are demarcated by the region within the thick black contours.

phases of MJO during December–February (Shinoda et al., 2016; Yoneyama and Zhang, 2020). These studies suggest dominant signatures of the intraseasonal oscillations (30–90-day signals) over the Maritime Continents representing the different phases of MJO. The 3rd – 5th phases of MJO are active over the strait during November–February (Wheeler and Hendon, 2004). The RMM index consists of a pair of normalized principal components (RMM1 and RMM2) derived from the combined EOF analysis of tropical outgoing longwave radiations and zonal winds. The RMM2 has been considered in this study to look into the intraseasonal oscillations associated with the MJO events, representing the active phases of MJO (3rd – 5th phases) propagating over the Maritime Continents. Owing to unavailability of daily chlorophyll-a data, the monthly chlorophyll-a data has been extensively used in this study, which makes it a bit difficult to investigate the variabilities at the intraseasonal time scale. Thus, an indirect evidence of the possible intraseasonal relationship between RMM2 and chlorophyll-a is established in this study using the rectified wavelet analysis technique (Liu et al., 2007). Since, the conventional wavelet power spectrum is known to be biased towards low frequencies (Torrence and Compo, 1998), the wavelet power spectrum is rectified by dividing the squared amplitude by its corresponding period (temporal scale) following Liu et al. (2007). This modified method leads to a substantial improvement in the spectral

estimate by removing the bias, thus allowing for a comparison of the spectral peaks across different temporal scales. Fig. 7d and e represent the rectified wavelet power spectra and the corresponding global wavelet spectra of the chlorophyll-a and RMM2 index. In the MS, significant annual cycles with highest amplitudes are observed in both chlorophyll-a and RMM2 index. It is evident that the highest chlorophyll-a values are observed every year during December–February, whenever MJO propagates over the domain during its 3rd – 5th phase (Fig. 7d and e). Also, the spatial correlation of the RMM2 index with the chlorophyll-a during 2007–2018 indicates an in-phase relationship with MJO events (with a maximum correlation of 0.48,  $p$ -value  $< 0.001$ ) (Fig. 7c). Thus, it can be indirectly inferred that the peak values of chlorophyll-a during December–February are closely linked to the active phases of the MJO events over the strait than those of the IOD and ENSO events.

To summarize, the higher wind stress associated with the active phase of MJO events in November induced coastal upwelling leads to high chlorophyll-a blooming along the west coast of Malaysia. The NEM strengthens during December–February leading to intense wind-induced coastal upwelling and wind stress curl-induced upwelling in the strait, well supported by the spatial distribution of SST. The chlorophyll-a bloom subsequently reduces during March associated with a

significant decrease in the wind stress.

On the other hand, significant downwelling features associated with lower chlorophyll-a concentration, reduced coastal upwelling, and negative wind stress curl along with higher SST, have been observed during the SWM in the north of the strait. Thus, it can be hypothesized that the stronger winds associated with the MJO events during December–February leads to the intense chlorophyll-a blooms and generation of the chlorophyll-a “tongue” in the MS through Ekman dynamics.

## 6. Summary and conclusions

This study focuses on investigating the factors responsible for higher chlorophyll-a concentration during the boreal winter (during December–February) in the MS and dynamics associated with the evolution of a “chlorophyll-a” tongue using the remote sensing satellite datasets during 2007–2018. Also, the role of the climatic events on the long-term chlorophyll-a variability is investigated in the strait.

The seasonal variability of chlorophyll-a concentration is apparent in the strait with a threefold increase in amplitude during the NEM (December–February), compared to SWM (May–September). Prominent signatures of concurrent thermocline doming are apparent from the subsurface temperature and salinity variations at the seasonal time scale. The seasonal variability of chlorophyll-a is strongly correlated with the meridional component of Ekman mass transport, SST, and local wind stress curl, with SSHA playing a limited supportive role through a cyclonic eddy. Stronger north-easterlies during the active phases of the MJO events during December–February have induced intense coastal upwelling along the west coast of Malaysia, resulting in higher chlorophyll-a concentration in the strait. The upwelling phenomena in the MS are further supported by positive wind stress curl-induced Ekman pumping and the entrainment of the subsurface cold and saline waters during the entire NEM. The evolution of the chlorophyll-a “tongue” in the domain is primarily due to the higher wind stress-induced north-westward Ekman mass transport ( $M_y$ ) and enhanced by local upwelling. The spatial distribution of SST significantly characterizes the distribution of chlorophyll-a in the domain. Also, the peak river discharge can bring in nutrient-rich waters from the land in the MS during December–January and can also contribute to the higher chlorophyll-a content. The nutrient waters with high chlorophyll-a concentration induced by coastal upwelling are carried by Ekman transport and gets advected north-westward from the west coast of Malaysia.

Limited studies have focused on the variability of chlorophyll-a concentration in the MS, and hence the possible mechanisms that regulate the local chlorophyll-a variability are unknown. The higher wind stress-induced Ekman pumping seems to be in phase with the high chlorophyll-a concentration during the NEM. Although the domain of the study is limited to the MS, the intraseasonal oscillations associated with the MJO play a vital role in enhancing the chlorophyll-a concentration during the NEM. Thus, the study can be extended to the entire coverage of the Maritime Continents and Indonesian Seas to see the possible impact of the strong and weak MJO events in future studies. Biological productivity also depends upon the light intensity in the euphotic zone and nutrient distribution both horizontally and vertically. Hence, setting up a regional model and performing numerical experiments would help determine the relative importance of such processes. Also, the results of the present study can be vital towards planning field experiments or research cruise to determine the relative contribution of wind stress and the influx from the rivers.

## Declaration of Competing Interest

The authors declare that they have no known competing financial interests or personal relationships that could have appeared to influence the work reported in this paper.

## Acknowledgments

The altimeter products are produced by SSALTO/DUACS and well distributed by AVISO with support from CNES. The MODIS Chlorophyll data are provided by the Ocean Ecology Laboratory, Ocean Biology Processing Group at the NASA Goddard Space Flight Centre through the NASA Ocean Biology Distributed Active Archive Centre. R. Dwi Susanto is supported by NASA grants 80NSSC18K0777 and NNX17AE79A through the University of Maryland, College Park. The authors highly acknowledge and thank the editor and anonymous reviewers for their comprehensive suggestions and encouraging comments. All the figures are generated in MatLab.

## References

- Aldrian, E., Susanto, R.D., 2003. Identification of three dominant rainfall regions within Indonesia and their relationship to sea surface temperature. *Int. J. Climatol.* 23, 1435–1452.
- Chang, C.P., Harr, P.A., Chen, H.J., 2005. Synoptic disturbances over the equatorial South China Sea and western maritime continent during boreal winter. *Mon. Weather Rev.* 133, 489–503.
- Chaturvedi, N., Narain, A., Pandey, P.C., 1998. Remote sensing applications in oceanography with special reference to biophysical coupling: a review. *Indian J. Marine Sci.* 27, 1–9.
- Chelton, D.B., Gaube, P., Schlax, M.G., Early, J.J., Samelson, R.M., 2020. The influence of nonlinear mesoscale eddies on near-surface oceanic chlorophyll. *Science* 334, 328–332.
- Chen, H., Malanotte-Rizzoli, P., Koh, T.Y., Song, G., 2014. The relative importance of the wind-driven and tidal circulations in Malacca Strait. *Cont. Shelf Res.* 88, 92–102.
- Haditjar, Y., Putri, M.R., Ismail, N., Muchlisin, Z.A., Rizal, S., 2019. Numerical simulation of currents and volume transport in the Malacca Strait and part of South China Sea. *Engl. J.* 23 (6) <https://doi.org/10.4186/ej.2019.23.6.129>.
- Hii, Y.S., Law, A.T., Shazili, N.A.M., Rashid, M.K.A., Lokman, H.M., Yusoff, F.M., Ibrahim, H.M., 2006. The strait of Malacca: hydrological parameters, biological oxygen demand and total suspended solids. *J. Sustain. Sci. Manag.* 1, 1–14.
- Ibrahim, Z.Z., Yanagi, T., 2006. The influence of the Andaman Sea and the South China Sea on water mass in the Malacca Strait. *La Mer* 43, 33–42.
- Isa, N.S., Akhri, M.F., Kok, P.H., Daud, N.R., Khalil, I., Roseli, N.H., 2020. Spatial and temporal variability of sea surface temperature during El-Niño southern oscillation and Indian Ocean dipole in the strait of Malacca and Andaman Sea. *Reg. Stud. Mar. Sci.* 39, 101402.
- Jana, S., Gangopadhyay, A., Chakraborty, A., 2015. Impact of seasonal river input on the bay of Bengal simulation. *Cont. Shelf Res.* 104, 45–62.
- Joo, T.L., Samah, A.A., 2004. *Weather and Climate of Malaysia*. University of Malaya Press, pp. 1–170.
- Liu, Y., Liang, X.S., Weisberg, R.H., 2007. Rectification of the bias in the wavelet power spectrum. *J. Atmos. Ocean. Technol.* 24 (12), 2093–2102. <https://doi.org/10.1175/2007JTECHO511.1>.
- Mandal, S., Sil, S., Shee, A., Swain, D., Pandey, P.C., 2018a. Comparative analysis of SCATSat-1 gridded winds with buoys, ASCAT, and ECMWF winds in the bay of Bengal. *IEEE J. Select. Topics Appl. Earth Observ. Remote Sens.* 11 (3), 845–851.
- Mandal, S., Sil, S., Shee, A., Venkatesan, R., 2018b. Upper Ocean and subsurface variability in the bay of Bengal during cyclone ROANU: a synergistic view using in situ and satellite observations. *Pure Appl. Geophys.* 175, 4605–4624.
- Mandal, S., Sil, S., Gangopadhyay, A., Jena, B.K., Venkatesan, R., Gawarkiewicz, G., 2020. Seasonal and tidal variability of surface currents in the Western Andaman Sea using HF radars and buoy observations during 2016–2017. *IEEE Trans. Geosci. Remote Sens.* <https://doi.org/10.1109/TGRS.2020.3032885>.
- Pang, W.C., Tkalic, P., 2003. Modeling tidal and monsoon driven currents in the Singapore Strait. *Singap. Marit. Port J.* 2003, 151–162.
- Rao, R.R., Girishkumar, M.S., Ravichandran, M., Rao, A.R., Gopalakrishna, V.V., Thadathil, P., 2010. Interannual variability of kelvin wave propagation in the wave guides of the equatorial Indian Ocean, the coastal bay of Bengal and the southeastern Arabian Sea during 1993–2006. *Deep-Sea Res.* 1 57 (1), 1–13.
- Rizal, S., 2000. The role of non-linear terms in the shallow water equation with the application in three-dimensional tidal model of the Malacca Straits and Taylor’s problem in low geographical latitude. *Cont. Shelf Res.* 20, 1965–1991.
- Rizal, S., Setiawan, I., Iskandar, T., Ilhamsyah, Y., Wahid, M.A., Musman, M., 2010. Currents simulation in the Malacca Straits by using three-dimensional numerical model. *Sains Malaysiana* 39, 519–524.
- Rizal, S., Damm, P., Wahid, M.A., Sundermann, J., Ilhamsyah, Y., Iskandar, T., Muhammad, 2012. General circulation in the Malacca Strait and Andaman Sea: a numerical model study. *Am. J. Environ. Sci.* 8, 479–488.
- Salahuddin, A., Scott, C., 2011. Climate extremes in Malaysia and the equatorial South China Sea. *Glob. Planet. Chang.* 78, 83–91.
- Setiawan, R.Y., Setyobudi, E., Wirasatriya, A., Muttaqin, A.S., Maslukah, L., 2019. The influence of seasonal and interannual variability on surface chlorophyll-a off the Western lesser Sunda Islands. *IEEE J. Select. Topics Appl. Earth Observ. Remote Sens.* 12 (11), 4191–4197.
- Setiawan, R.Y., Wirasatriya, A., Hernawan, U., Leung, S., Iskandar, I., 2020. Spatio-temporal variability of surface chlorophyll-a in the Halmahera Sea and its relation to ENSO and the Indian Ocean dipole. *Int. J. Remote Sens.* 41 (1), 284–299.

- Shinoda, T., Han, W., Jensen, T.G., Zamudio, L., Metzger, E.J., Lien, R.C., 2016. Impact of the madden-julian oscillation on the Indonesian throughflow in the Makassar strait during the CINDY/DYNAMO field campaign. *J. Clim.* 29, 6085–6108.
- Siswanto, E., Tanaka, K., 2014. Phytoplankton biomass dynamics in the strait of Malacca within the period of the SeaWiFS full Mission: seasonal cycles, interannual variations and decadal-scale trends. *Remote Sens.* 6, 2718–2742.
- Susanto, R.D., Wei, Z., Adi, R.T., Fan, B., Li, S., Fang, G., 2013. Observations of the Karimata Strait throughflow from December 2007 to November 2008. *Acta Oceanol. Sin.* 32, 1–6.
- Tan, C.K., Ishizaka, J., Matsumura, S., Yusoff, F.M., Mohamed, M.I.H., 2006. Seasonal variability of SeaWiFS chlorophyll a in the Malacca Straits in relation to Asian monsoon. *Cont. Shelf Res.* 26 (2), 168–178.
- Torrence, C., Compo, G.P., 1998. A practical guide to wavelet analysis. *Bull. Am. Meteorol. Soc.* 79, 61–78.
- Van Maren, D.S., Gerritsen, H., 2012. Residual flow and tidal asymmetry in the Singapore Strait, with implications for resuspension and residual transport of sediment. *J. Geophys. Res.* 117, C04021.
- Wang, Y., Xu, T., Li, S., Susanto, R.D., Agustiadi, T., Trenggono, M., Tan, W., Wei, Z., 2019. Seasonal variation of water transport through the Karimata Strait. *Acta Oceanol. Sin.* 38, 47–57.
- Wei, Z., Li, S., Susanto, R.D., Wang, Y., Fan, B., Xu, T., Sulistiyo, B., Adi, T.R., Setiawan, A., Kuswardani, A., Fang, G., 2019. An overview of 10-year observation of the South China Sea branch of the Pacific to Indian Ocean throughflow at the Karimata Strait. *Acta Oceanol. Sin.* 38 (4), 1–11.
- Wheeler, M., Hendon, H.H., 2004. An all-season real-time multivariate MJO index: development of an index for monitoring and prediction. *Mon. Weather Rev.* 132, 1917–1932.
- Wirasatriya, A., Setiawan, J.D., Sugianto, D.N., Rosyadi, I.A., Haryadi, H., Winarso, G., Setiawan, R.Y., Susanto, R.D., 2020. Ekman dynamics variability along the southern coast of Java revealed by satellite data. *Int. J. Remote Sens.* 41 (21), 8475–8496.
- Wrytki, K., 1961. Physical oceanography of the southeast Asian waters. In: NAGA Report No. 2. University California, pp. 1–195.
- Yoneyama, K., Zhang, C., 2020. Years of the maritime continent. *Geophys. Res. Lett.* 47 (e2020GL087182).